Transport of an optically generated electron-hole plasma in a semiconductor slab: Approach to stationarity

T. Held, T. Kuhn,* and G. Mahler
Institut für Theoretische Physik, Universität Stuttgart, Pfaffenwaldring 57, D-7000 Stuttgart 80, Federal Republic of Germany
(Received 20 October 1989)

The perpendicular transport of an optically generated ambipolar electron-hole plasma is investigated in a semiconductor slab. Under the condition of high carrier-carrier scattering rates, a hydrodynamical description with heated and displaced Maxwellians is possible. The transition of the system into its stationary state is examined with respect to the validity of an effective one-component approximation. Scattering mechanisms implying different ratios of momentum and energy relaxation rates are found to induce different spatial profiles of hydrodynamical variables.

I. INTRODUCTION

The ambipolar transport of optically generated carriers in semiconductors has been investigated in a series of experiments.[1-5] Under low excitations it has been possible to explain the results in terms of isothermal diffusion.[2,3,5] In these cases the transport is dominated by excitons. In other cases, however, additional degrees of freedom appeared to be necessary to fit theoretical calculations to measured data. Steranka and Wolfe[1] have introduced a phonon wind to explain their experiments, while Tsen and Sankey[4] have included a high drift velocity for fitting. In previous papers[6,7] (cited hereafter as I and II, respectively) the importance of a varying carrier temperature has finally been demonstrated, which can even induce reverse diffusion, i.e., a particle current density directed towards increasing density. These investigations were carried out with an effective one-component system under stationary conditions using a kinetic description.

On the other side there are a lot of theoretical[8-11] and experimental[12-16] studies on carrier cooling in homogeneous systems of various dimensionality. The theoretical investigations cover the range from electron-hole interaction[9] to nonequilibrium phonon effects.[8,10] However, in most cases a spatial transport is not considered.

In paper II it has been shown that the heated and displaced Maxwellian (HDM) model is a good approximation for high electron-electron scattering rates. Within this approach we now investigate a two-component system with more-detailed scattering terms than retained in a relaxation-time approximation. These scattering terms depend in a nontrivial way on the hydrodynamic variables and differ with respect to momentum and energy relaxation.

In this paper we investigate the approach of an electron-hole plasma to its stationary state addressing the question, on which length and time scales an effective one-component approximation should be valid. Further on we examine the influence of the more-detailed scattering terms on the profiles of the hydrodynamic variables of our system.

II. THE HDM MODEL

The semiconductor sample we investigate is an $Al_xGa_{1-x}As$ slab, constrained in one dimension (the z direction) and having large extensions in both lateral directions. At the boundaries, surface recombination is taken into account. The material properties of the slab are homogeneous. A laser beam is oriented perpendicularly to the slab and enters the crystal at $z=0$. The light is absorbed generating carriers at a rate g_c independent of the lateral directions and with excess energies determined by the laser frequency. Density and temperature gradients then induce transport effects. Various scattering mechanisms lead to momentum and energy relaxation of the carriers.

We assume that the phonons remain in their equilibrium state and thus act as a heat bath. Then, for the dynamics of our system we only have to consider the electrons and holes. The kinetic description of an electron-hole plasma consists of two Boltzmann equations coupled by electron-hole scattering and by the Poisson equation for the electric field, **E**. In the slab geometry, spatial inhomogeneities occur only in the z direction. Therefore we get one-dimensional (with respect to spatial variables) Boltzmann equations for the distribution functions f_e and f_h, respectively, and a one-dimensional Poisson equation for E_z:

$$\frac{\partial}{\partial t}f_c(z,\mathbf{v},t)+v_z\frac{\partial}{\partial z}f_c(z,\mathbf{v},t)+\frac{q_cE_z}{m_c}\frac{\partial}{\partial v_z}f_c(z,\mathbf{v},t) = g_c(z,\mathbf{v},t)+\left[\frac{\partial f}{\partial t}\right]_c^{\text{coll}}, \quad c=e,h \; ; \tag{1}$$

$$\frac{\partial}{\partial z}E_z=\frac{q_h}{\epsilon_0\epsilon_r}(n_h-n_e) \; . \tag{2}$$

Here $\mathbf{v}$ is the respective carrier velocity, n_c the carrier density, ϵ_r the background dielectric function, q_c the carrier charge, and m_c the effective carrier mass.

For simplicity we assume parabolic bands. The generation term g_c is due to the photons of the laser. A

recombination may occur either in the bulk or at the surface. The quotient between slab width and surface recombination velocity (a hydrodynamical characterization of the surface quality) sets a time scale: If this time is smaller than the bulk lifetime of the carriers, the bulk recombination is negligible in comparison to the surface recombination. This condition is fullfilled in our case because of high surface recombination velocities[17] in (Al)GaAs and small layer width. The scattering term [second one on the right-hand side of Eq. (1)] consists of three terms: carrier-lattice scattering, electron-hole scattering, and electron-electron, or hole-hole scattering, respectively. In the case of high carrier-carrier scattering rates compared to carrier-lattice scattering rates we can approximate the two distribution functions f_c by heated and displaced Maxwellians:

$$f_c(z,\mathbf{v},t)=\frac{n_c(z,t)}{2}\left[\frac{2\pi m_c}{k_B T_c(z,t)}\right]^{3/2} \times\exp\left[-\frac{m_c[\mathbf{v}-v_c(z,t)\mathbf{e}_z]^2}{2k_B T_c(z,t)}\right] . \tag{3}$$

Here $\mathbf{e}_z$ is the unit vector in z direction. These Maxwellians are parametrized by their first three moments, the carrier density n_c, the drift velocity v_c, and the temperature T_c:

$$n_c(z,t)=\frac{1}{4\pi^3}\int f_c(z,\mathbf{v},t)\,d^3v, \quad c=e,h \ ; \tag{4a}$$

$$v_c(z,t)\mathbf{e}_z=\frac{1}{n_c(z,t)}\frac{1}{4\pi^3}\int \mathbf{v} f_c(z,\mathbf{v},t)\,d^3v \ ; \tag{4b}$$

$$\frac{k_B T_c(z,t)}{m_c}=\frac{1}{3n_c(z,t)}\frac{1}{4\pi^3} \times\int(\mathbf{v}-v_c(z,t)\mathbf{e}_z)^2 f_c(z,\mathbf{v},t)\,d^3v \ . \tag{4c}$$

Inserting Eq. (3) into the Boltzmann equation (1) and constructing the three moments [analogous to Eq. (4)] we obtain six hydrodynamic equations for n_e, n_h, v_e, v_h, T_e, and T_h. If the electric forces are strong enough they will induce local charge neutrality, which means equal densities of electrons and holes and—due to charge conservation—equal drift velocities. We eliminate the electric field and get the following equations for an ambipolar electron-hole plasma:

$$\frac{\partial}{\partial t}n+\frac{\partial}{\partial z}nv=G^{(0)}, \quad c=e,h \ ; \tag{5a}$$

$$\frac{\partial}{\partial t}v+\frac{\Theta_e+\Theta_h}{n}\frac{\partial}{\partial z}n+v\frac{\partial}{\partial z}v+\frac{\partial}{\partial z}(\Theta_e+\Theta_h) =\frac{1}{n}(J^{(1)}-vG^{(0)}) \ ; \tag{5b}$$

$$\frac{\partial}{\partial t}\Theta_c+\frac{2}{3}\Theta_c\frac{\partial}{\partial z}v+v\frac{\partial}{\partial z}\Theta_c =\frac{1}{3n}(J_c^{(2)}+G_c^{(2)}-3\Theta_c G^{(0)}) \ ; \tag{5c}$$

where we use the following abbreviations:

$$\Theta_c=\frac{k_B T_c}{m_e+m_h} , \tag{6}$$

$$G^{(0)}=\frac{1}{4\pi^3}\int g_e\,d^3v=\frac{1}{4\pi^3}\int g_h\,d^3v =\frac{\alpha P(t)}{\hbar\omega_L}e^{-\alpha z} , \tag{7a}$$

$$G_c^{(2)}=\frac{m_c}{m_e+m_h}\frac{1}{4\pi^3}\int(\mathbf{v}-v_c\mathbf{e}_z)^2 g_c\,d^3v =\frac{m_c G^{(0)}}{m_e+m_h}\left[\frac{E_{\text{exc}}}{2\left[\frac{1}{m_e}+\frac{1}{m_h}\right]m_c^2}+v_c^2\right] , \tag{7b}$$

$$J^{(1)}=J_e^{(1)}+J_h^{(1)} , \tag{8a}$$

$$J_c^{(1)}=\frac{m_c}{m_e+m_h}\frac{1}{4\pi^3}\int v_z\left[\frac{\partial f}{\partial t}\right]_c^{\text{coll}} d^3v , \tag{8b}$$

$$J_c^{(2)}=\frac{m_c}{m_e+m_h}\frac{1}{4\pi^3}\int(\mathbf{v}-v_c\mathbf{e}_z)^2\left[\frac{\partial f}{\partial t}\right]_c^{\text{coll}} d^3v \ . \tag{8c}$$

E_{exc} is the excess energy, $\hbar\omega_L$ the photon energy, α^{-1} the absorption length, and $P(t)$ the laser power density.

To solve Eq. (5) we need initial and boundary conditions for the four hydrodynamic variables. The initial conditions depend on the scenario and will be discussed in Sec. IV. Two boundary conditions are given by the surface recombination velocities which are the values of the drift velocities at the two surfaces. Close to the boundaries the hydrodynamic drift velocity is not the true mean velocity of the carriers (in gas dynamics, the difference between a kinetic and a hydrodynamic calculation specifies the so-called Knudsen layer), but rather the recombination velocity.[18] In the stationary case (see paper II) the remaining boundary condition is an algebraic relation between carrier temperature and density at the zero point of the drift velocity. In our time-dependent case we have two differential relations between each Θ_c and n. We refer to Appendix A for a more detailed discussion.

III. SCATTERING RATES

For the HDM model the electron-electron and hole-hole scattering terms vanish, so that only two types of scattering mechanisms remain, electron-hole scattering and carrier-lattice scattering. They drive the hydrodynamic variables to their respective equilibrium values. For electron-hole scattering this equilibrium is the state with both carrier temperatures being equal; the drift velocities are always the same in the ambipolar approach. The equilibrium of carrier-lattice scattering is reached if the common drift velocity vanishes and the carriers have lattice temperature.

The lattice scattering mechanisms can be divided into two categories, interaction with static disorder (impurities, alloy) and interaction with dynamic disorder (phonons). The scattering with a static defect is elastic, while the phonon scattering mechanisms contribute to momen-

tum relaxation as well as to energy relaxation. From interaction with phonons we only have to take into account the acoustic-deformation-potential scattering and the polar optic scattering. Piezoelectric scattering is negligible,[19] the optical-deformation-potential scattering is vanishing for parabolic bands, and the excess energy we use is so low that intervalley scattering does not play any role. We assume that the static defects are reduced to the technologically possible minimum: no dislocations and impurities being of low density and partially compensated. Thus we only need to consider alloy scattering and ionized impurity scattering, while neutral-impurity and space-charge scattering are negligible.

According to Eq. (8) we calculate the first ($\nu=1$) and second ($\nu=2$) moment of the scattering term. The detailed calculation is given in Appendix B. We introduce scattering times $\tau_{ci}^{(\nu)}$ by

$$J_c^{(1)}=-\frac{m_c}{m_e+m_h}n(z,t)\,v(z,t)\sum_i\frac{1}{\tau_{ci}^{(1)}(n,v,T_c)}\,,\qquad c=e,h\;; \tag{9a}$$

$$J_c^{(2)}=-n(z,t)3[\Theta_c(z,t)-\Theta_L]\sum_i\frac{1}{\tau_{ci}^{(2)}(n,v,T_c)}-2v_cJ_c^{(1)}\,. \tag{9b}$$

Θ_L is expressed analogously to Eq. (6) with carrier temperature T_c replaced by lattice temperature T_L.

The total scattering times depend on the hydrodynamic variables and material parameters. In Fig. 1 the dependence on the carrier temperature and the aluminum fraction is plotted. The momentum relaxation time shows a sensitive dependence on the aluminum fraction x. This fact is due to alloy scattering, which is the dominating momentum relaxation mechanism for higher values of x. A strong temperature dependence can be seen for the energy relaxation times. At lower temperatures the carriers cannot emit optical phonons because of energy conservation. Thus the scattering time rises until the acoustic-deformation-potential scattering dominates.

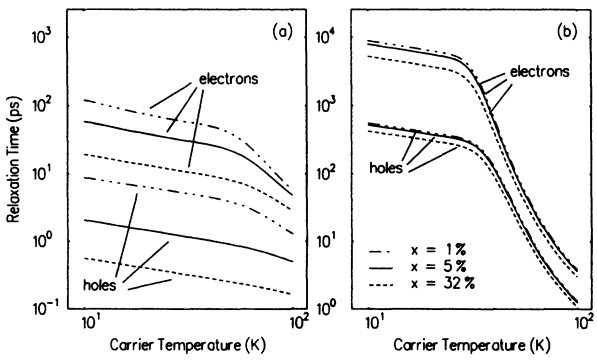

FIG. 1. Total momentum (a) and energy (b) relaxation time in $Al_xGa_{1-x}As$ as a function of the carrier temperature. Hydrodynamic parameters: $n=10^{16}$ cm^{-3}, $v=10^5$ cm/s. Doping: $N_D=7\times10^{14}$ cm^{-3}, $N_A=3\times10^{14}$ cm^{-3}. Lattice temperature: $T_L=10$ K. Material parameters as in Refs. 5, 22, and 23.

A weak dependence on the aluminum fraction is due to the varying effective mass. Comparing the values of momentum and energy relaxation times we recognize in some temperature regions a difference of several decades according to the high aluminum concentration. This fact will be important for the discussion in Sec. V.

We treat electron-hole scattering similarly to carrier-lattice scattering and obtain (see Appendix B):

$$J_{c,eh}^{(2)}=-n(z,t)3[\Theta_c(z,t)-\Theta_{c'}(z,t)]\times\frac{1}{\tau_{eh}^{(2)}(n,v,T_e,T_h)}\,,\quad c,c'=e,h;c\neq c'\,. \tag{10}$$

Due to the two-particle nature of electron-hole scattering, the scattering time depends strongly on carrier density.

IV. ROLE OF ELECTRON-HOLE SCATTERING

The scenario we investigate now is the transition of our system into its stationary state after the laser [used in the continuous-wave (cw) mode] is switched on at a time $t=0$. The values of the hydrodynamic variables at this time define our initial conditions. In the beginning the cold equilibrium carriers, due to the background doping, dominate over the newly generated hot carriers. Thus the mean internal energy per carrier (described in terms of a temperature) is low. But with increasing number of carriers the temperature is also increasing, predominantly in the generation region. Due to their small mass compared to the hole mass, the electrons get the main part of the excess energy, and thus a higher temperature. On the one hand, the temperature is increasing outside the generation region because of the onset of transport, on the other hand the scattering with the phonons reduces the temperature again. At later times we see that electron and hole temperatures are nearly identical, at least outside the generation region, but still far from equilibrium with the lattice. The reason for this is the electron-hole scattering. It becomes stronger with increasing carrier density until it is the dominant scattering mechanism and rapidly reduces the difference between electron and hole temperatures (see Fig. 2).

This temperature difference as a measure for nonequilibrium between the carrier species is the subject we will investigate now in more detail. As we see in Fig. 3 the maximum of this nonequilibrium measure shifts to later times for increasing distance from the generation region. This is due to the transport of the electron-hole plasma. The absolute height of the maximum is decreasing because carrier-lattice scattering reduces both carrier temperatures. The most important fact is that the temperature difference at the latest point in time is nearly 2 orders of magnitude smaller than at its overall maximum value.

To investigate the role of the electron-hole scattering we vary the laser power. Higher power means higher generation rates. This leads to an enlarged number of carriers and thus to a higher electron-hole scattering rate. In Fig. 4 we see that the temperature difference is decreasing with increasing laser power, as expected. But it

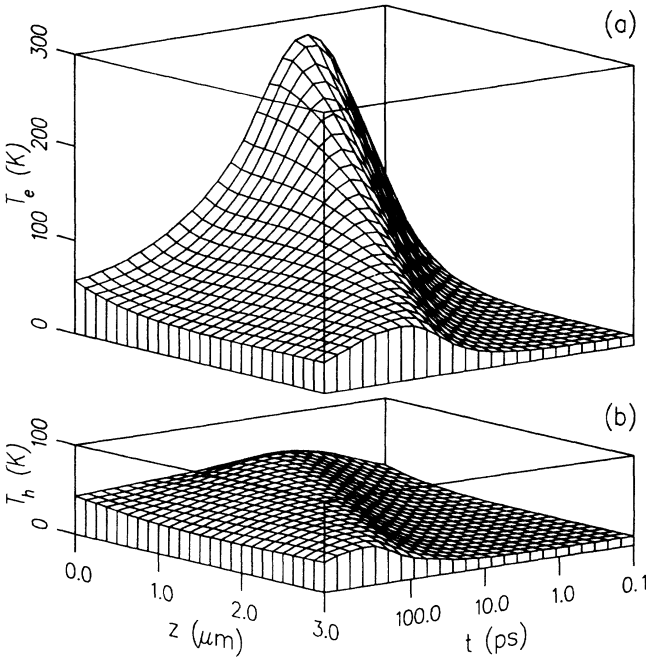

FIG. 2. Spatial and temporal evolution of electron (a) and hole (b) temperature. Slab width $L=3$ μm. $s_o=s_L=10^5$ cm/s. $x=32\%$. Other parameters as in Fig. 1. Laser excess energy $E_{\text{exc}}=125$ meV. Laser power $P_L=20$ W mm^{-2}.

is not possible to reduce the difference to arbitrarily small values by continuously increasing the power, because in the case of very high densities, the screening of the carriers reduces the efficiency of electron-hole scattering. We also recognize in Fig. 4 that the temperature difference in the generation region is higher than in the rest of the slab because the laser permanently creates new nonequilibrium. But the temperature difference in the generation region is still small compared to the maximum values at the beginning of the excitation, as shown in Fig. 3.

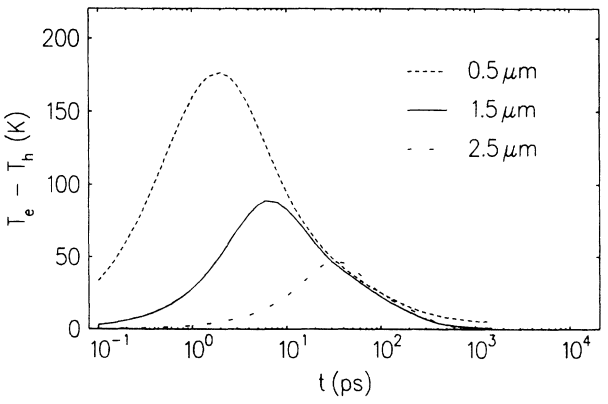

FIG. 3. Temporal behavior of the temperature nonequilibrium at different positions. Parameters as in Fig. 2.

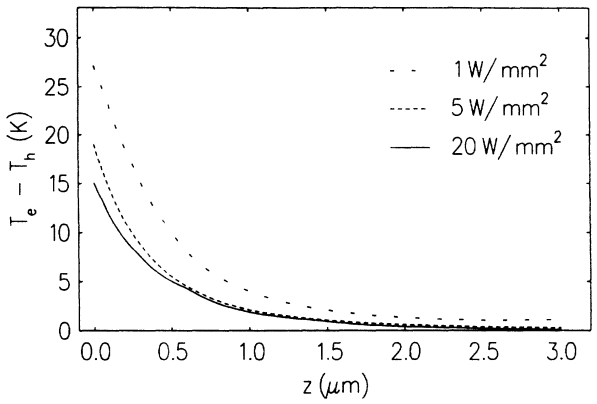

FIG. 4. Spatial behavior of the nonequilibrium under different laser powers at $t=1.5$ ns. Parameters as in Fig. 2.

V. EFFECTIVE ONE-COMPONENT SYSTEM

In Sec. IV we have studied the electron-hole nonequilibrium. In the effective one-component approach, electrons and holes are assumed to have the same density, drift and temperature. From Eq. (5) we get

$$\frac{\partial}{\partial t}n+\frac{\partial}{\partial z}nv=G^{(0)}\,, \tag{11a}$$

$$\frac{\partial}{\partial t}v+\frac{\Theta}{n}\frac{\partial}{\partial z}n+v\frac{\partial}{\partial z}v+\frac{\partial}{\partial z}\Theta=\frac{1}{n}(J^{(1)}-vG^{(0)})\,, \tag{11b}$$

$$\frac{\partial}{\partial t}\Theta+\frac{2}{3}\Theta\frac{\partial}{\partial z}v+v\frac{\partial}{\partial z}\Theta=\frac{1}{3n}(J^{(2)}+G^{(2)}-3\Theta G^{(0)})\,, \tag{11c}$$

with the abbreviations

$$\Theta=\Theta_e+\Theta_h=\frac{2k_BT}{m_e+m_h}\,, \tag{12a}$$

$$J^{(2)}=J_e^{(2)}+J_h^{(2)}\,, \tag{12b}$$

$$G^{(2)}=G_e^{(2)}+G_h^{(2)}\,. \tag{12c}$$

To examine the validity of the one-component approximation we consider the transition into the stationary state as shown in Fig. 5. The hydrodynamic variables of the one- and of the two-component systems have a different time behavior, especially in the beginning of the excitation, but in the stationary state they are quite similar. We have chosen a point outside the generation region and far away from the boundaries of the slab. As described in the last section we also recognize the equality of the electron and hole temperatures as soon as the density is high enough to ensure dominating electron-hole scattering. What is remarkable is that velocity and temperature reach their stationary values earlier than the density, because the time scale for the density dynamics, given by generation and transport, is longer than the time scales for the other variables, which are directly governed by the relaxation times.

As previously shown (see I and II) a striking feature in

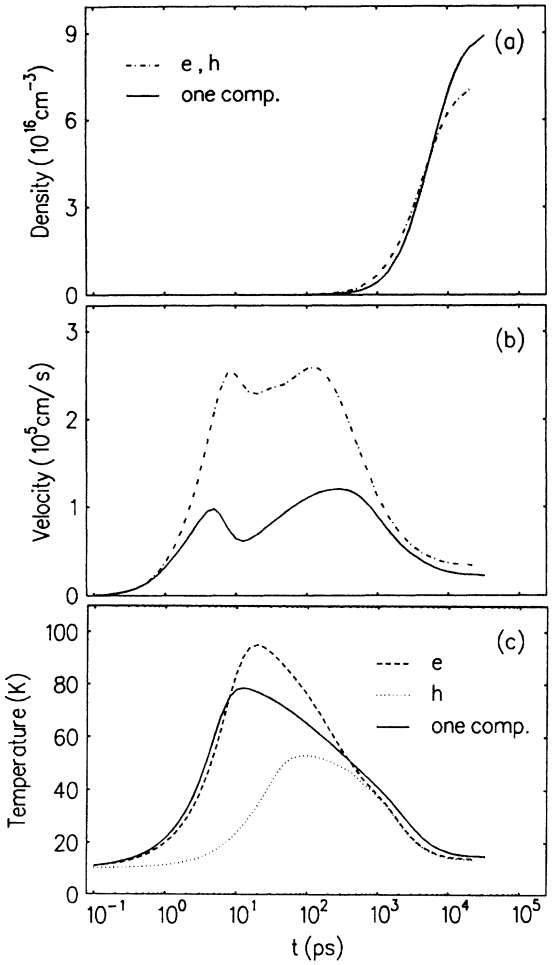

FIG. 5. Temporal evolution of the hydrodynamic variables of an electron-hole plasma and an effective one-component system at $z=2$ μm. Parameters as in Fig. 2.

the stationary state beyond isothermal diffusion is the possible occurrence of reverse diffusion: In addition to a density gradient, a high temperature gradient may also induce a current. If the generation does not supply this current with enough carriers, the current produces a density gradient with the same sign as the current. Related to this density gradient is a velocity overshoot. We examine now the influence of a difference between momentum and energy relaxation times. Therefore we vary the aluminum fraction. It effect on the alloy scattering and thus on the momentum relaxation allows us to vary the ratio of those relaxation times. The stationary profiles shown in Fig. 6 demonstrate that the reverse diffusion and thus the velocity overshoot are most pronounced if momentum and energy relaxation times are of the same order of magnitude ($\tau^{(1)} \approx \tau^{(2)}$), this being the case for low aluminum fractions, as we see in Fig. 1. For higher aluminum concentrations, the momentum relaxation is much faster than the energy relaxation ($\tau^{(1)} \ll \tau^{(2)}$). In this case the effect of the temperature gradient, i.e., the particle current, is counterbalanced by the pronounced momentum relaxation, leading to a reduced velocity overshoot. Under the same conditions two distinct regions of different density and temperature gradients can be seen in Fig. 6, reflecting the temperature dependence of the relaxation ratio, an effect which becomes smaller with decreasing aluminum fraction. With a constant ratio (equal to 1 in papers I and II) only a single region results. Close to the left boundary we recognize a third small region of differing density gradient, especially for the 20% curve, which is due to the carrier capture of the surface.

VI. CONCLUSIONS

We have investigated the transport of an ambipolar electron-hole plasma within the HDM approximation. The spatial and temporal behavior of this system after switching on a laser allows us to draw two conclusions: First of all, the one-component approximation is valid for stationary problems. It is supported by higher carrier densities because of the influence of the electron-hole scattering. A measure of validity of this approximation is the difference between electron and hole temperatures.

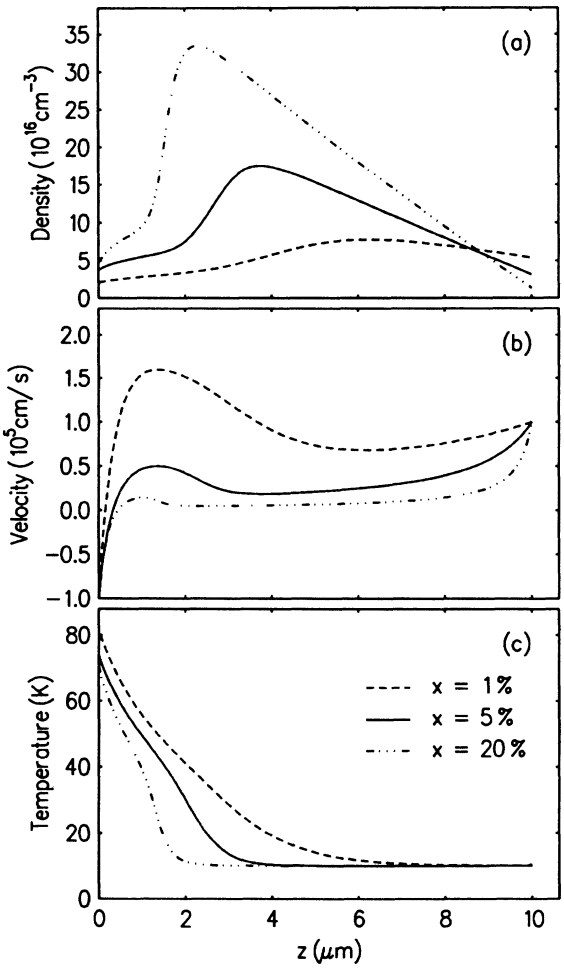

FIG. 6. Stationary state of the effective one-component system in $Al_xGa_{1-x}As$ with various aluminum fractions. Slab width $L=10$ μm. Laser excess energy $E_{exc}=250$ meV. Other parameters as in Fig. 2.

The spatial variance of this measure is small compared to the temporal variance during the approach to the stationary state. Secondly, the reverse diffusion as an effect of nonisothermal diffusion is most pronounced if momentum and energy relaxation times are of the same order of magnitude.

ACKNOWLEDGMENTS

The authors would like to thank K. Scheller for valuable discussions. This work has been supported by the Deutsche Forschungsgemeinschaft (Bonn, Germany) under Grant No. Ma-614/5-2.

APPENDIX A

As we mentioned in Sec. II the boundary conditions are not obvious. For a practicable handling of Eq. (5) we introduce the new variables $\mathbf{j}=n\mathbf{v}$ (particle current density) and $b_c=n^{-2/3}\Theta_c$ instead of v and Θ_c. The transformed equation system reads

$$\frac{\partial}{\partial t}n+\frac{\partial}{\partial z}j=G^{(0)} ,$$

$$\frac{\partial}{\partial t}j+\left[\frac{5}{3}(b_e+b_h)n^{2/3}-\left[\frac{j}{n}\right]^2\right]\frac{\partial}{\partial z}n + \frac{2j}{n}\frac{\partial}{\partial z}j+n^{5/3}\frac{\partial}{\partial z}(b_e+b_h)=J^{(1)} ,$$

$$\frac{\partial}{\partial t}b_c+\frac{j}{n}\frac{\partial}{\partial z}b_c=\tfrac{1}{3}n^{-5/3}(J_c^{(2)}+G_c^{(2)}-3n^{2/3}b_cG^{(0)}) .$$

At the point with vanishing j the equations for the b_c are ordinary differential equations and can be solved with the known initial conditions. The thereby-calculated values for the b_c are used as boundary conditions for the areas left and right of this point. The surface recombination velocities at the left ($z=0$) and right ($z=L$) margin of the sample form the boundary conditions for the n and j equations:

$$\frac{j}{n-n_0}\Big|_{z=0}=s_0 \quad \text{and} \quad \frac{j}{n-n_0}\Big|_{z=L}=s_L .$$

APPENDIX B

The scattering term can be interpreted as a balance of transition between various electronic states. Such a state is characterized by spin $\mathbf{S}$ and wave vector $\mathbf{k}$. The latter is in our case proportional to the velocity $\mathbf{v}$ so that we can use this variable as before. For the carrier-lattice scattering we get

$$\left[\frac{\partial f}{\partial t}\right]^{\text{coll}}=\sum_{\mathbf{k}',\mathbf{s}'}[W(\mathbf{k}'(\mathbf{v}'),\mathbf{S}'\rightarrow\mathbf{k}(\mathbf{v}),\mathbf{S})f(\mathbf{v}') - W(\mathbf{k}(\mathbf{v}),\mathbf{S}\rightarrow\mathbf{k}'(\mathbf{v}'),\mathbf{S}')f(\mathbf{v})] .$$

We neglect a filling of the final states, which is consistent with a HDM model. The transition probabilities are given by Fermi's golden rule (for elastic scattering $\omega_q=0$):

$$W(\mathbf{k}',\mathbf{S}'\rightarrow\mathbf{k},\mathbf{S}) = \frac{2\pi}{\hbar}\sum_{\pm}|\langle\mathbf{k}|H_1|\mathbf{k}'\rangle|^2\delta(E_{\mathbf{k}'}-E_{\mathbf{k}}\pm\hbar\omega_q)\delta_{ss'} .$$

The matrix elements of the interaction Hamiltonian are taken from Ref. 20. According to Eq. (8) the moments of the scattering term are calculated. For the acoustic-deformation-potential scattering this calculation is performed in Ref. 21. The scattering times for the different mechanisms introduced in Eq. (9) are given by the following formulas.

Acoustic-deformation-potential scattering:

$$\frac{1}{\tau_{\text{ad}}^{(1)}}=2\left[\frac{2}{\pi}\right]^{3/2}\frac{E_{1c}^2m_c^2}{\hbar^4\rho_0u_{\text{lo}}}k_BT_c\frac{1}{\beta^3}\exp\left[-\frac{\beta^2}{2}\right]\int_0^\infty\xi\frac{\cosh[(\gamma_1-\gamma_2)\xi]}{\sinh(\gamma_1x)}\exp\left[-\frac{\xi^2}{2}\right][\beta\xi\cosh(\beta\xi)-\sinh(\beta\xi)]dx ,$$

$$\frac{1}{\tau_{\text{ad}}^{(2)}}=\frac{4}{3}\left[\frac{2}{\pi}\right]^{3/2}\frac{E_{1c}^2m_c^{5/2}}{\hbar^4\rho_0}\frac{1}{\beta\left[1-\dfrac{T_L}{T_c}\right]}\exp\left[-\frac{\beta^2}{2}\right]\int_0^\infty\xi^2\frac{\sinh[(\gamma_1-\gamma_2)\xi]}{\sinh(\gamma_1\xi)}\exp\left[-\frac{\xi^2}{2}\right]\sinh(\beta\xi)d\xi .$$

Polar optic scattering:

$$\frac{1}{\tau_{\text{po}}^{(1)}}=\frac{k_B\Theta_{\text{op}}}{\pi^{3/2}\hbar^2}\left[\frac{m_c}{2k_BT_c}\right]^{1/2}\frac{e^2}{\epsilon_0}\left[\frac{1}{\epsilon_r(\infty)}-\frac{1}{\epsilon_r(0)}\right]\frac{1}{\beta^3}\frac{\cosh(\Omega_L-\Omega)}{\sinh(\Omega_L)} \times\int_0^\infty\frac{\xi^2}{(\xi^2+\Lambda^{-2})^2}\exp\left[-\frac{1}{2}\left[\frac{\Omega}{\xi}\right]^2\right]\exp\left[-\frac{\xi^2}{2}\right][\beta\xi\cosh(\beta\xi)-\sinh(\beta\xi)]d\xi ,$$

$$\frac{1}{\tau_{\text{po}}^{(2)}}=\frac{(k_B\Theta_{\text{op}})^2m_c^{1/2}}{3\sqrt{2}(\pi k_BT_c)^{3/2}\hbar^2}\frac{e^2}{\epsilon_0}\left[\frac{1}{\epsilon_r(\infty)}-\frac{1}{\epsilon_r(0)}\right]\frac{1}{\beta\left[1-\dfrac{T_L}{T_c}\right]}\frac{\sinh(\Omega_L-\Omega)}{\sinh(\Omega_L)} \times\int_0^\infty\frac{\xi^2}{(\xi^2+\Lambda^{-2})^2}\exp\left[-\frac{1}{2}\left[\frac{\Omega}{\xi}\right]^2\right]\exp\left[-\frac{\xi^2}{2}\right]\sinh(\beta\xi)d\xi .$$

Alloy scattering:

$$\frac{1}{\tau^{(1)}_{\text{alloy}}}=3\left[\frac{m_c}{2}\right]^{3/2}\frac{x(1-x)}{\hbar^4 N_A}\Delta E_c^2(\pi k_B T_c)^{1/2}\left[\frac{1}{\beta^2}\exp\left[-\frac{\beta^2}{2}\right]+\left[\frac{\pi}{2}\right]^{1/2}\frac{\beta^2-1}{\beta^3}\Phi\left[\frac{\beta}{\sqrt{2}}\right]\right],$$

$$\frac{1}{\tau^{(2)}_{\text{alloy}}}=0\ .$$

Impurity scattering:

$$\frac{1}{\tau^{(1)}_{\text{imp}}}=\frac{N_{\text{I}}}{m_c^{1/2}(2\pi k_B T_c)^{3/2}}\left[\frac{e^2}{\epsilon_0\epsilon_r}\right]^2\frac{1}{\beta^3}\exp\left[-\frac{\beta^2}{2}\right]\int_0^\infty\frac{\exp\left[-\frac{\xi^2}{2}\right]}{(\xi^2+\Lambda^{-2})^2}[\beta\xi\cosh(\beta\xi)-\sinh(\beta\xi)]d\xi\ ,$$

$$\frac{1}{\tau^{(2)}_{\text{imp}}}=0\ .$$

We have used the following abbreviations:

$$\beta=\left[\frac{m_c v^2}{k_B T_c}\right]^{1/2},\quad \gamma_1=u_{\text{lo}}\left[\frac{m_c}{k_B}\right]^{1/2}\frac{T_c^{1/2}}{T_L},\quad \gamma_2=u_{\text{lo}}\left[\frac{m_c}{k_B}\right]^{1/2}\frac{1}{T_c^{1/2}},$$

$$\Omega=\frac{k_B\Theta_{\text{op}}}{2k_B T_c},\quad \Omega_L=\frac{k_B\Theta_{\text{op}}}{2k_B T_L},\quad \lambda_D^{-2}=\frac{e^2 n}{\epsilon_0\epsilon_r k_B}\left[\frac{1}{T_e}+\frac{1}{T_h}\right],\quad \Lambda^{-2}=\lambda_D^{-2}\frac{\hbar^2}{4m_c k_B T_c}\ .$$

As defined in Ref. 20, E_{1c} is the acoustic-deformation-potential parameter, ρ_0 the crystal density, u_{lo} the longitudinal sound velocity, $k_B\Theta_{\text{op}}$ the energy of the longitudinal optical phonons, N_A the number of atoms in the crystal, ΔE_c the alloy scattering potential, and N_I the density of ionized impurities. The numerical values are taken from Refs. 5, 22, and 23.

We treat electron-hole scattering in the same way. The balance for two-particle scattering is

$$\left[\frac{\partial f}{\partial t}\right]^{\text{coll}}=\sum_{\substack{\mathbf{k}_2,\mathbf{k}_1',\mathbf{k}_2',\\ S_2,S_1',S_2'}}W(\mathbf{k}_1,\mathbf{k}_2,S_1,S_2\rightarrow\mathbf{k}_1',\mathbf{k}_2',S_1',S_2')[f_e(\mathbf{v}_1')f_h(\mathbf{v}_2')-f_e(\mathbf{v}_1)f_h(\mathbf{v}_2)]\ ,$$

with the transition probability

$$W=\frac{2\pi}{\hbar}|\langle\mathbf{k}_1'|H_I|\mathbf{k}_1\rangle|^2\delta_{\mathbf{k}_1+\mathbf{k}_2,\mathbf{k}_1'+\mathbf{k}_2'}\delta(E_{\mathbf{k}_1}+E_{\mathbf{k}_2}-E_{\mathbf{k}_1'}-E_{\mathbf{k}_2'})\delta_{S_1,S_2}\delta_{S_1',S_2'}\ .$$

Analogous to the calculations in case of carrier-lattice scattering we get the scattering time

$$\frac{1}{\tau^{(2)}_{\text{eh}}}=\frac{n}{3(2\pi)^{5/2}k_B^{3/2}m_e m_h\left[\frac{T_e}{m_e}+\frac{T_h}{m_h}\right]^{3/2}}\left[\frac{e^2}{\epsilon_0\epsilon_r}\right]^2\int_0^\infty\frac{\xi^3}{(\xi^2+\Lambda^{-2})^2}\exp\left[-\frac{\xi^2}{2}\right]d\xi\ ,$$

$$\Lambda^{-2}=\lambda_D^{-2}\frac{\hbar^2}{4k_B\left[\frac{1}{m_e}+\frac{1}{m_h}\right]^{-2}\left[\frac{T_e}{m_e}+\frac{T_h}{m_h}\right]}\ ,$$

with the screening length λ_D as defined above.

---

*Present address: Dipartimento di Fisica, Università degli Studi di Modena, via Campi 213/A, I-41100 Modena, Italy.

[1]F. M. Steranka and J. P. Wolfe, Phys. Rev. B **34**, 1014 (1986).

[2]J. C. Culbertson, R. M. Westervelt, and E. E. Haller, Phys. Rev. B **34**, 6980 (1986).

[3]G. Mahler, T. Kuhn, A. Forchel, and H. Hillmer, in *Optical Nonlinearities and Instabilities in Semiconductors,* edited by H. Haug (Academic, San Diego, 1988), p. 159.

[4]K. T. Tsen and O. F. Sankey, Phys. Rev. B **37**, 4321 (1988).

[5]H. Hillmer, A. Forchel, S. Hansmann, M. Morohashi, E. Lopez, H. P. Meier, and K. Ploog, Phys. Rev. B **39**, 10901 (1989).

[6]T. Kuhn and G. Mahler, Phys. Rev. B **35**, 2827 (1987).
[7]T. Kuhn and G. Mahler, Phys. Rev. B **39**, 1194 (1989).
[8]M. Asche and O. G. Sarbei, Phys. Status Solidi B **141**, 487 (1987).
[9]M. Osman and D. K. Ferry, J. Appl. Phys. **61**, 5330 (1987).
[10]W. Pötz, Phys. Rev. B **36**, 5016 (1987).
[11]A. Kabasi, D. Chattopadhyay, and C. K. Sarkar, J. Appl. Phys. **65**, 1598 (1989).
[12]R. F. Leheny, J. Shah, R. L. Fork, C. V. Shank, and A. Migus, Solid State Commun. **31**, 809 (1979).
[13]J. F. Ryan, R. A. Taylor, A. J. Turberfield, A. Maciel, J. M. Worlock, A. C. Gossard, and W. Wiegmann, Phys. Rev. Lett. **53**, 1841 (1984).
[14]J. Shah, A. Pinczuk, A. C. Gossard, and W. Wiegmann, Phys. Rev. Lett. **54**, 2045 (1985).
[15]J. Collet, J. L. Oudar, and T. Amand, Phys. Rev. B **34**, 5443 (1986).
[16]R. A. Höpfel, J. Shah, P. A. Wolff, and A. C. Gossard, Phys. Rev. B **37**, 6941 (1988).
[17]L. Jastrzebski, J. Lagowski, and H. C. Gatos, Appl. Phys. Lett. **27**, 537 (1975).
[18]T. Kuhn and G. Mahler, Phys. Rev. B **40**, 12 147 (1989).
[19]A. Saxena, Phys. Rev. B **24**, 3295 (1981).
[20]L. Reggiani, in *Hot-Electron Transport in Semiconductors,* Vol. 58 of *Topics in Applied Physics,* edited by L. Reggiani (Springer, Berlin, 1985), p. 66.
[21]A. C. Baynham, P. N. Butcher, W. Fawcett, and J. M. Loveluck, Proc. Phys. Soc. **92**, 783 (1967).
[22]D. E. Aspnes, S. M. Kelso, R. A. Logan, and R. Bhat, J. Appl. Phys. **60**, 754 (1986).
[23]K. F. Brennan, D. H. Park, K. Hess, and M. A. Littlejohn, J. Appl. Phys. **63**, 5004 (1988).